EUROPEAN ORGANIZATION FOR NUCLEAR RESEARCH

CERN-PPE/91-162
30 September, 1991

A Measurement of the W and Z Production Cross Sections and a Determination of Γ_W at the CERN $\overline{p}p$ Collider

The UA2 Collaboration

Bern - Cambridge - CERN - Dortmund - Heidelberg - Melbourne -
Milano - Orsay (LAL) - Pavia - Perugia - Pisa - Saclay (CEN)

J. Alitti[12], G. Ambrosini[9], R. Ansari[8], D. Autiero[11], P. Bareyre[12], I. A. Bertram[6], G. Blaylock[3,a], P. Bonamy[12], K. Borer[1], M. Bourliaud[12], D. Buskulic[8], G. Carboni[11], D. Cavalli[7], V. Cavasinni[11], P. Cenci[10], J. C. Chollet[8], C. Conta[9], G. Costa[7], F. Costantini[11], L. Cozzi[7], A. Cravero[7], M. Curatolo[11], A. Dell'Acqua[9], T. DelPrete[11], R. S. DeWolf[2], L. DiLella[3], Y. Ducros[12], G. F. Egan[6], K. F. Einsweiler[3,b], B. Esposito[11], L. Fayard[8], A. Federspiel[1], R. Ferrari[9], M. Fraternali[9,c], D. Froidevaux[3], G. Fumagalli[9], J. M. Gaillard[8], F. Gianotti[7], O. Gildemeister[3], C. Gössling[4], V. G. Goggi[9], S. Grünendahl[5], K. Hara[1,d], S. Hellman[3], J. Hřivnáč[3], H. Hufnagel[4], E. Hugentobler[1], K. Hultqvist[3,e], E. Iacopini[11,f], J. Incandela[7], K. Jakobs[3], P. Jenni[3], E. E. Kluge[5], N. Kurz[5], S. Lami[11], P. Lariccia[10], M. Lefebvre[3], L. Linssen[3], M. Livan[9,g], P. Lubrano[3,10], C. Magneville[12], L. Mandelli[7], L. Mapelli[3], M. Mazzanti[7], K. Meier[3,h], B. Merkel[8], J. P. Meyer[12], M. Moniez[8], R. Moning[1], M. Morganti[11,i], L. Müller[1], D. J. Munday[2], M. Nessi[3], F. Nessi-Tedaldi[3], C. Onions[3], T. Pál[1], M. A. Parker[2], G. Parrour[8], F. Pastore[9], E. Pennacchio[9], J. M. Pentney[3], M. Pepe[3], L. Perini[7,c], C. Petridou[11], P. Petroff[8], H. Plothow-Besch[3], G. Polesello[3,9], A. Poppleton[3], K. Pretzl[1], M. Primavera[11,j], M. Punturo[10], J. P. Repellin[8], A. Rimoldi[9], M. Sacchi[9], P. Scampoli[10], J. Schacher[1], B. Schmidt[4], V. Šimák[3], S. L. Singh[2], V. Sondermann[4], R. Spiwoks[4], S. Stapnes[3], C. Talamonti[10], F. Tondini[10], S. N. Tovey[6], E. Tsesmelis[4], G. Unal[8], M. Valdata-Nappi[11,j], V. Vercesi[9], A. R. Weidberg[3,k], P. S. Wells[2,ℓ], T. O. White[2], D. R. Wood[8], S. A. Wotton[2,ℓ], H. Zaccone[12], A. Zylberstejn[12]

(submitted to Phys. Lett. B)

Abstract

The decays $W \to e\nu$ and $Z \to e^+e^-$ are studied in $\bar{p}p$ collisions at $\sqrt{s} = 630$ GeV. The products of production cross section and branching ratio are measured as $\sigma^e_W = 682 \pm 12 \pm 40$ pb and $\sigma^e_Z = 65.6 \pm 4.0 \pm 3.8$ pb. The results are in good agreement with $O(\alpha_s^2)$ calculations of the production cross sections. Many systematic effects cancel in the ratio, $R = 10.4 \pm^{0.7}_{0.6} \pm 0.3$, which can be used to give an indirect measurement of the total width of the W boson: $\Gamma_W = 2.10 \pm 0.13 \pm 0.09$ GeV. The width gives a limit on the top quark mass, $m_{top} > 53$ GeV (95% CL), which is independent of the top decay mode.

[1]Laboratorium für Hochenergiephysik, Universität Bern, Sidlerstraße 5, 3012 Bern, Switzerland
[2]Cavendish Laboratory, University of Cambridge, Cambridge, CB3 0HE, UK
[3]CERN, 1211 Geneva 23, Switzerland
[4]Lehrstuhl für Exp. Physik IV, Universität Dortmund, 4600 Dortmund, FRG
[5]Institut für Hochenergiephysik der Universität Heidelberg, Schröderstraße 90, 6900 Heidelberg, FRG
[6]School of Physics, University of Melbourne, Parkville 3052, Australia
[7]Dipartimento di Fisica dell'Università di Milano and Sezione INFN Milano, 20133 Milano, Italy
[8]Laboratoire de l'Accélérateur Linéaire, Université de Paris-Sud, 91405 Orsay, France
[9]Dipartimento di Fisica Nucleare e Teorica, Università di Pavia and INFN, Sezione di Pavia, Via Bassi 6, 27100 Pavia, Italy
[10]Dipartimento di Fisica dell'Università di Perugia and INFN, Sezione di Perugia, Via Pascoli, 06100 Perugia, Italy
[11]Dipartimento di Fisica dell'Università di Pisa and INFN Sezione di Pisa, Via Livornese, S. Piero a Grado, 56100 Pisa, Italy
[12]Centre d'Etudes Nucléaires de Saclay, 91191 Gif-sur-Yvette Cedex, France
a) Now at University of California, Santa Cruz, USA
b) Now at Lawrence Berkeley Laboratory, Berkeley, California, USA
c) Now at Istituto di Fisica, Università di Palermo, Italy
d) Now at University of Tsukuba, Tsukuba, Ibaraki 305, Japan
e) Now at University of Stockholm, Stockholm, Sweden
f) Also at Scuola Normale Superiore, Pisa, Italy
g) Now at Dipartimento di Fisica, Università di Cagliari, Italy
h) Now at Deutsches Elektronen Synchrotron, Hamburg, FRG
i) Now at Dipartimento di Fisica e INFN di Bologna, Università di Bologna, Italy
j) Now at Dipartimento di Fisica dell'Università della Calabria e gruppo INFN, Cosenza, Italy
k) Now at Nuclear Physics Laboratory, University of Oxford, Oxford, UK
ℓ) Now at CERN, Geneva, Switzerland

1 Introduction

In a hadron collider, the clearest signatures for W and Z production are given by their leptonic decays. The upgraded UA2 experiment is optimized for the identification of electrons and the indirect detection of neutrinos through the measurement of missing transverse momentum, so the decays $W \rightarrow e\nu$ and $Z \rightarrow ee$ give the most precise estimate of the production rates. An earlier measurement of the products of cross section times branching ratio, $\sigma^e_W = \sigma(\bar{p}p \rightarrow W + X)B(W \rightarrow e\nu)$ and $\sigma^e_Z = \sigma(\bar{p}p \rightarrow Z + X)B(Z \rightarrow e^+e^-)$, based on data taken in 1988-89 [1] is improved with the additional statistics from the 1990 run of the CERN $\bar{p}p$ collider. The measurements of σ^e_W and σ^e_Z can be compared to recent theoretical predictions which include complete $O(\alpha_s^2)$ calculations of the production cross sections [2].

In addition, one can obtain a measurement of the ratio of total widths of the W and Z (Γ_Z/Γ_W) from the ratio $R = \sigma^e_W/\sigma^e_Z$. Given the precise determination of Γ_Z from LEP data, the measurement of R at hadron colliders gives the best determination of Γ_W. The W total width is an interesting probe of the Standard Model, and in particular it is sensitive to any additional decay modes of the W regardless of whether or not they are observable. For example, this measurement can be used to establish a lower limit on the mass of the top quark which is independent of the manner in which the top decays.

2 The UA2 Apparatus

The UA2 detector was substantially upgraded between 1985 and 1987. Reference [1] contains a summary of the features of the apparatus relevant to the study of W and Z bosons, and only the major points are repeated here. Additional details about specific detector elements can be found in the references given below.

The central calorimeter [3] covers a pseudorapidity (η) range of $-1 < \eta < 1$ while the end cap calorimeters complete the coverage out to $-3 < \eta < 3$. The same technique (lead and iron absorber plates with scintillator and wavelength shifter readout) is used throughout. An electromagnetic compartment of 17.0-24.4 radiation lengths (depending on polar angle) with lead absorber plates is followed by hadronic compartments with iron absorber plates. In the central calorimeter, the hadronic region is subdivided in depth into two compartments of two interaction lengths each. The lateral segmentation in the central calorimeter is constant in azimuth (ϕ) and polar angle (θ) ($\Delta\phi = 15°$, $\Delta\theta = 10°$). In the end caps, the two cells closest to the beam axis ($2.5 < |\eta| < 3.0$ and $2.2 < |\eta| < 2.5$) cover 30° in azimuth, and the other cells have a constant segmentation $\Delta\phi = 15°$, $\Delta\eta = 0.2$. The electromagnetic compartments of the outermost cells of the central calorimeter (edge cells), which cover $0.8 < |\eta| < 1.0$, are trimmed to accommodate the inner detectors and consequently have a degraded performance.

Clusters are constructed in the calorimeter by joining all cells with an energy greater than 400 MeV sharing a common edge. Those clusters with a small lateral size and a small energy leakage into the hadronic compartments are marked as electromagnetic clusters and are subsequently examined as potential electron candidates.

Inside the central calorimeter is a series of nested cylindrical subdetectors. Around the beam pipe, at radii of 3.5 cm (inner) and 14.5 cm (outer), are two arrays of silicon pad

counters used for tracking and ionization measurements [4]. Between the two is a cylindrical drift chamber with jet geometry (the Jet Vertex Detector or JVD) [5]. Outside of the outer silicon layer is the Transition Radiation Detector (TRD) [6], consisting of two sets of radiators and drift chambers. The outermost of the central detectors is the Scintillating Fibre Detector (SFD) [7], which consists of approximately 60 000 fibres arranged on cylinders into 8 stereo triplets.

The last elements before the calorimeters are "preshower detectors", used to localize the early development of electromagnetic showers initiated in a lead converter. In front of the central calorimeter, this function is performed by the SFD, where 1.5 radiation lengths of lead are positioned before the last two stereo triplets of fibres. For the end cap region, tracking and preshower detection is accomplished by the End Cap Proportional Tubes (ECPT) [8]. In each case, an electron is identified by a dense cluster of charge in the preshower region (after the converter) which lies close to a reconstructed track [1].

For electron analyses, the detector can be logically divided into three acceptance regions, in which efficiency, rejection and resolution are studied separately: central (non-edge) ($|\eta| < 0.8$), central (edge) ($0.8 < |\eta| < 1.0$) and forward ($1.0 < |\eta| < 1.6$). The limits of the forward acceptance region for electrons are defined by the ECPT tracking and preshower volumes.

Collisions take place along the central axis of the detector, with an a *rms* spread along the beam direction of 130 mm. The minimum bias trigger signal is obtained from the Time of Flight counters (TOF), and the luminosity is measured using eight scintillator telescopes at small angles to the beams. The instantaneous luminosity in 1990 was typically twice as large as in 1988-89, and the average for the complete data sample is 2.0 10^{30} cm^{-2}sec^{-1}. The average probability of having an extra minimum bias interaction accompanying a W or Z event is around 26% (18% in 1988-89 and 35% in 1990), but events with multiple interaction vertices are not discarded and only about 5% of W and Z events are lost due to vertex confusion.

3 Event Selection and Reconstruction

The data were collected from 1988 to 1990 at the CERN $\bar{p}p$ collider at an energy of $\sqrt{s} = 630$ GeV, and represent the complete sample of the upgraded UA2 experiment. After removing events in which not all of the detector elements used in this analysis were functioning, the integrated luminosity is 13.0 ± 0.7 pb^{-1}. Requirements are imposed in order to select events where $\bar{p}p \rightarrow W + X$, $W \rightarrow e\nu$ or $\bar{p}p \rightarrow Z + X$, $Z \rightarrow e^+e^-$.

3.1 Electron Identification

The electron identification procedure begins with criteria for the calorimeter cluster and then combines information from the tracking and preshower detectors. The steps are described here briefly and the efficiency of each cut is given in Table 1. The procedure is described in detail in ref. [1] along with the methods for evaluating the efficiencies. Most components of the efficiency are measured using the W sample itself, and the results in Table 1 correspond to the full statistics. In some cases, the higher average luminosity and detector

Table 1: Electron selection efficiencies.

	Central Region		Forward Region
	non-edge	edge	
Calorimeter (trigger level)	$91.7 \pm 0.7\%$	$91.8 \pm 1.6\%$	$95.9 \pm 0.8\%$
Calorimeter (χ^2)	$93.8 \pm 0.8\%$	$91.6 \pm 2.3\%$	$94.6 \pm 1.5\%$
Track-Preshower (standard)	$77.2 \pm 1.7\%$		$94.7 \pm 1.8\%$
Track-Preshower (loose)	$97.9 \pm 1.2\%$		
Total (standard)	$66.4 \pm 2.0\%$	$64.9 \pm 3.3\%$	$85.9 \pm 1.7\%$
Total (loose)	$84.2 \pm 1.5\%$	$82.4 \pm 3.0\%$	

aging have resulted in a decrease in efficiency with respect to the subsample of 1988-89 data reported previously.

The identification of electromagnetic clusters is obtained from calorimeter information alone. The lateral size of the shower and the leakage into the hadronic compartment must both be small. Cuts on these quantities are applied at the trigger level, and the efficiency of these cuts includes the effects due to accidental overlap with particles from the underlying event which can spoil the electron cluster profile.

A standard electron candidate must also have a track reconstructed in the tracking detectors which points to an electromagnetic cluster in the calorimeter. The track must originate from a reconstructed vertex which is not displaced more than 250 mm along the beam direction from the centre of the detector. Furthermore, a preshower cluster must be reconstructed which is consistent with the position of the electron candidate track. In addition, a set of looser electron cuts is defined for the region covered by the central calorimeter, in order to recover electrons for which either the track or the preshower cluster is not correctly reconstructed by the standard pattern recognition algorithms. In such cases, SFD data from the vicinity of the electron candidate are examined, and cuts are made directly on the number of layers hit in the tracking region or on the charge detected in the preshower layers [1].

Once the precise track trajectory is known, a χ^2 test is used to require that the lateral and longitudinal profile of the shower in the calorimeter is consistent with that expected from an electron incident along that trajectory as measured in test beams.

The detected energy is summed in a small number (typically two or three) of calorimeter cells which are assigned to the electron. Energy corrections are applied according to the precise electron direction and impact point in the calorimeter based on data obtained from 40 GeV test beam electrons. The corrected energy is used together with the direction given by the tracking detectors to define the electron momentum, $\vec{p}^{\,e}$.

The fiducial cuts are described in ref. [1]. In the central (non-edge) region, there are no explicit fiducial cuts. For the edge cells, the 20 mm closest to the calorimeter edge (1.7° in θ) are excluded because the efficiency is poorly determined in this region. In the forward region, the electron trajectory is required to pass through both the tracking and preshower portions of the ECPT detector, and a cut is made to remove electrons near one of the cell boundaries in ϕ. In addition, forward electron trajectories must not pass through the radiator of the central preshower detector.

3.2 Neutrino Identification

The presence of neutrinos in $W \to e\nu$ decays is deduced by measuring the electron energy and the energies of the particles (generally hadrons) recoiling against the W. The missing transverse momentum ($\not\!\!p_T$) is attributed to the undetected neutrino:

$$\vec{p}_T^{\,\nu} \equiv \vec{\not\!\!p}_T = -\vec{p}_T^{\,e} - \vec{p}_T^{\,had}. \tag{1}$$

Here, $\vec{p}_T^{\,e}$ is the reconstructed transverse momentum of the electron candidate and $\vec{p}_T^{\,had}$ is the total transverse momentum of the recoil particles, calculated as

$$\vec{p}_T^{\,had} = \left(\sum E_{cell}\hat{v}_{cell}\right)_T, \tag{2}$$

where $\hat{v}_{cell}$ is a unit vector from the interaction vertex to the centre of a calorimeter cell, E_{cell} is the energy in that cell, and the sum extends over all cells in the calorimeter ($-3 < \eta < 3$) excluding the cells assigned to the electron.

3.3 Selection Requirements

All events must have an electron passing the standard identification cuts [1] with $p_T^e > 20$ GeV. This same requirement is placed on the W electron and at least one of the Z electrons so that one obtains a partial cancellation of the systematic errors in the ratio R.

The additional requirements for a W candidate are that $p_T^\nu > 20$ GeV and $m_T > 40$ GeV, where $m_T \equiv \sqrt{2p_T^e p_T^\nu(1 - cos\phi^{e\nu})}$ and $\phi^{e\nu}$ is the azimuthal separation between the measured electron and neutrino directions. The p_T^e, p_T^ν, and m_T spectra of the final sample are shown in Fig. 1. The kinematic effects of the different acceptance regions are quite clear; distributions for the central samples show more prominent Jacobian peaks, while the forward electrons produce much more flat distributions.

Z candidates require an additional electron with $p_T^e > 15$ GeV. This electron may pass the looser cuts described earlier. The invariant mass spectrum of the electron pairs (m_{ee}) selected in this way is shown in Fig. 2. The final sample of 269 events is obtained by requiring $76 < m_{ee} < 110$ GeV.

3.4 Backgrounds

The method for assessing the backgrounds is described in ref. [1]. The major background in the Z sample is QCD two-jet events in which the jets are misidentified as electrons. The rejection of jets is measured from the Z triggers (with the p_T cuts relaxed to 5.5 GeV on each cluster). By comparing the numbers of events with zero, one, and two clusters passing electron identification cuts in the region $40 < m_{ee} < 70$ GeV, the rejection power of the cuts against jets is measured along with the amounts of QCD and Drell-Yan events in that region. The background shape is extrapolated into the signal region, and the rejection factors then give an estimate of the background of 3.4 ± 0.3 events.

The QCD background in the W events arises when a jet is misidentified as an electron and the total p_T in the event is mismeasured so as to give an apparently large $\not\!\!p_T$. This background is estimated by comparing the $\not\!\!p_T$ spectrum of events with electron candidates

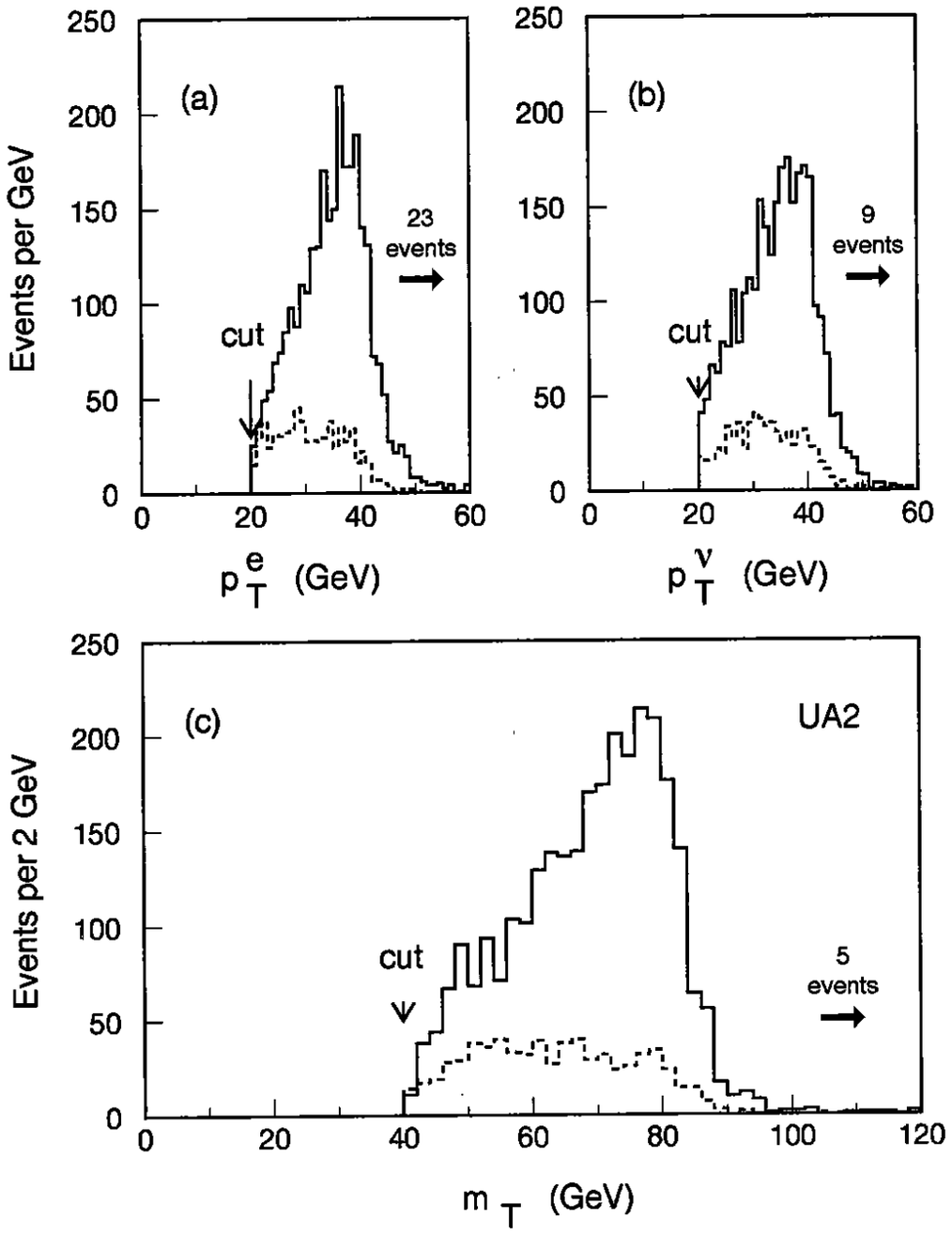

Figure 1: The p_T^e (a) and p_T^ν(b) and m_T (c) spectra for W candidates in the central (solid) and forward (dashed) acceptance regions.

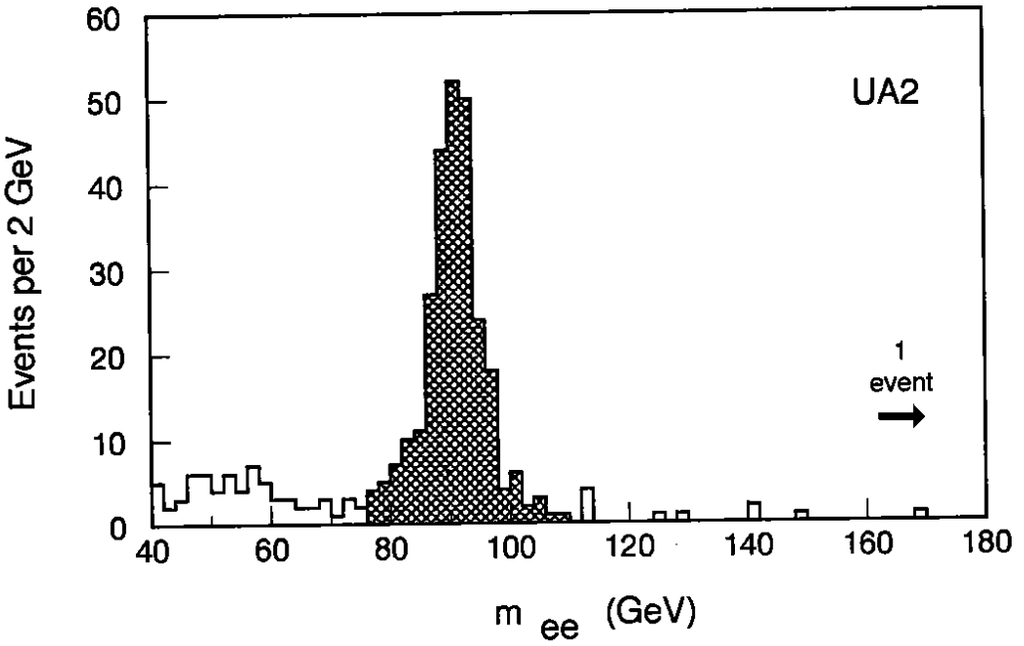

Figure 2: The invariant mass spectrum of electron pairs passing final identification cuts. The range of m_{ee} used to select the final Z candidates is indicated by the shaded region. The overflow event at $m_{ee} = 278$ GeV is discussed in ref. [1].

from the inclusive electron trigger (with no $\not{p}_T$ cut) to the same spectrum for π^0 candidates. The background surviving the final cuts is determined to be $0.5 \pm 0.2\%$ of the W candidates [9]. In addition, there is a background from the process $W \to \tau\nu$, $\tau \to e\nu\bar{\nu}$. This is estimated from Monte Carlo to be $3.8 \pm 0.1\%$ ($3.3 \pm 0.3\%$) in the central (forward) region.

4 Cross Section Calculation

The W cross section is computed in each acceptance region according to the formula

$$\sigma_W^e = \frac{N_W - N_{QCD} - N_\tau}{\epsilon\ \eta\ L} \tag{3}$$

where N_W is the number of W candidates observed, N_{QCD} is the estimated QCD background and N_τ is the estimated contribution from $W \to \tau\nu$. The geometrical acceptance η is calculated with the Monte Carlo model described in ref. [1]. The uncertainty on the acceptance is dominated by the choice of structure function sets because these can alter the rapidity distribution of the gauge bosons.

The measurement of the integrated luminosity (L) is discussed in ref. [1]. Note that for ρ, the ratio of the real to imaginary part of the forward scattering amplitude, the value used is that reported by the UA4 experiment, $\rho = 0.24 \pm 0.04$ [10]. Dispersion theory suggests $\rho = 0.15$ [11], which would correspond to cross sections 4.2% larger than the values reported here. If future measurements of ρ differ from the previously measured value, a correction to the following cross sections is required.

The quantity ϵ is the total efficiency, which is a product of the electron efficiency for the acceptance region and the global event efficiency, which consists of several factors. These include the vertex position cut efficiency (0.943 ± 0.002) and vertex finding efficiency (0.948 ± 0.005), which is dominated by the effect of events with multiple interactions. A minimum bias coincidence from the TOF counters was required for W and Z triggers for 74% of the data taken, resulting in an average efficiency of 0.978 ± 0.005. The product is 0.875 ± 0.008, which must be multiplied by the electron efficiency for the appropriate acceptance region to obtain ϵ in equation 3.

The cross sections for Z production are calculated in a similar manner:

$$\sigma_Z^e = \frac{(N_Z - N_{QCD})(1 - f_{\gamma^*})}{\epsilon\ \eta\ L} \ . \tag{4}$$

The observed number of candidates is N_Z, the QCD background estimate is N_{QCD}, the acceptance is η, and the integrated luminosity is L. The correction constant $f_{\gamma^*} = 1.65\%$ compensates for the contribution from single photon exchange and $\gamma^* Z$ interference, so that the final result can be compared to predictions based on the Z propagator alone. The factor ϵ contains a global event efficiency along with the appropriate electron pair efficiency for the sub-sample.

The event efficiency for the Z sample contains all of the factors applied to W events with the addition of two correction factors. A factor of 1.000 ± 0.0015 is also applied to allow for a different vertex efficiency on W and Z events. This efficiency is measured from the W sample, but it could be different for Z events because of the presence of an additional charged track. A second factor of 1.01 ± 0.01 accounts for the difference in the influence of the recoiling hadrons on the efficiency for single electrons in W events and back-to-back electron pairs in Z events. The event efficiency for Z events is then 0.884 ± 0.013.

The radiative decays $W \to e\nu\gamma$ and $Z \to e^+e^-\gamma$ are taken into account in the acceptance calculation. Although the photons from these decays are sometimes detected, they are not used in computing p_T^e or m_{ee}, and the resulting losses are absorbed in the acceptance. The rates and kinematic distribution for the radiative decays are obtained from the a Monte Carlo based on ref. [12], and the detector response to photons is modeled as described in ref. [13].

The cross section results for each subsample are shown in Tables 2 and 3. The final cross sections are obtained by combining the results from the individual subsample with weights according to the product of acceptance and efficiency. These results are $\sigma_W^e = 682 \pm 12 \pm 40$ pb and $\sigma_Z^e = 65.6 \pm 4.0 \pm 3.8$ pb.

The results are compared with the theoretical predictions in Fig. 3. QCD corrections have been calculated up to $O(\alpha_s^2)$ [2], and give good agreement with the measurements. There is some sensitivity to the choice of structure functions. The curves have been obtained with the parton density parameterizations of HMRSB [14] and the shaded bands at the right sides of the figures show the range of variation over several structure function sets [15], including HMRSE [14], KMRSB0 [16], GRV [17] MT-E1, MT-S1, and MT-B1 [18]. The structure function uncertainties on σ_W^e are of similar size to the experimental errors and the second order corrections. The dependence on the top quark mass of σ_W^e and σ_Z^e comes from the top contribution to the total widths. This is discussed further in the next section.

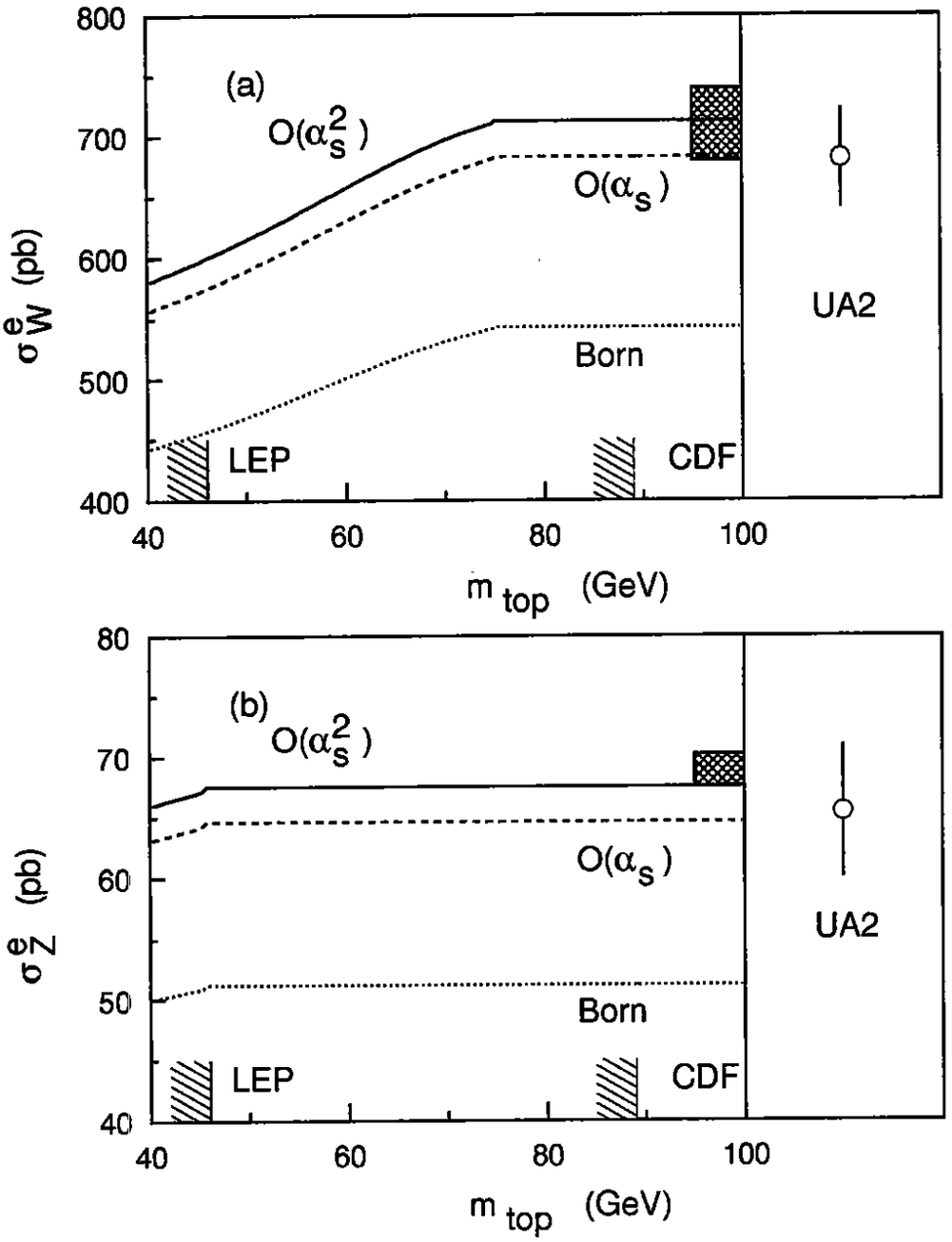

Figure 3: The measurements for σ_W^e (a) and σ_Z^e (b) are compared with the theoretical predictions as a function of the top quark mass at the Born level and including $O(\alpha_s)$ and $O(\alpha_s^2)$ corrections. The shaded bands at the right show the variation with structure functions. The top mass limits from LEP (model independent) and CDF (model dependent) are indicated on the abscissae.

Table 2: W cross section calculation.

Acceptance region	N_W	N_{QCD}	N_τ	η	σ_W^e (pb)
Central (non-edge)	2409	12.0 ± 4.8	91.5 ± 2.4	0.465 ± 0.016	$657 \pm 14 \pm 41$
Central (edge)	478	2.4 ± 1.0	18.2 ± 0.5	0.086 ± 0.003	$718 \pm 34 \pm 48$
Forward	672	11.4 ± 11.4	22.2 ± 2.0	0.086 ± 0.006	$758 \pm 31 \pm 54$
Combined	3559	25.8 ± 12.8	131.9 ± 3.5	0.639 ± 0.017	$682 \pm 12 \pm 40$

Table 3: Calculation of the Z cross section for the different subsamples. The electron acceptance regions are identified by Ce = Central (non-edge), Ed = Central (edge), Fd = Forward.

Acceptance region	N_Z	N_{QCD}	η	σ_Z^e (pb)
Ce-Ce	109	0.58 ± 0.09	0.200 ± 0.006	$68.6 \pm 6.6 \pm 4.4$
Ce-Ed	50	0.85 ± 0.15	0.093 ± 0.002	$68.3 \pm 9.9 \pm 4.6$
Ed-Ed	5	0.43 ± 0.11	0.010 ± 0.001	$60.3 \pm 29.8 \pm 5.7$
Ce-Fd	80	0.73 ± 0.16	0.152 ± 0.003	$61.6 \pm 7.1 \pm 3.9$
Ed-Fd	15	0.57 ± 0.15	0.030 ± 0.001	$57.4 \pm 15.6 \pm 4.3$
Fd-Fd	10	0.28 ± 0.09	0.016 ± 0.002	$70.0 \pm 23.8 \pm 8.1$
Combined	269	3.43 ± 0.31	0.502 ± 0.007	$65.6 \pm 4.0 \pm 3.8$

5 Cross Section Ratio and Γ_W

When one computes the ratio $R = \sigma_W^e/\sigma_Z^e$, the systematic errors are smaller than those on the individual cross sections. The luminosity errors cancel completely, and there are also large cancellations in the efficiency errors. The result is

$$R = 10.4 \pm^{0.7}_{0.6} (\text{stat}) \pm 0.3(\text{syst}) \tag{5}$$

where the correlations of all of the factors have been taken into account with a Monte Carlo error propagator to obtain the final errors.

Theoretically, this ratio can be expressed as

$$R = \frac{\sigma_W}{\sigma_Z} \frac{\Gamma(W \to e\nu)}{\Gamma(Z \to e^+e^-)} \frac{\Gamma_Z}{\Gamma_W} . \tag{6}$$

With some limited assumptions about the Standard Model, namely the standard gauge couplings of electrons, electron neutrinos, and light quarks, the first two ratios on the right hand size of equation (6) can be computed reliably. Table 4 shows the results of the computation for several sets of structure functions and values of Λ_{QCD}. The values of σ_W and σ_Z come from the $O(\alpha_s^2)$ calculation [2], where the mass values $m_W = 80.14 \pm 0.27$ GeV [13, 19] and $m_Z = 91.175 \pm 0.021$ [20] are assumed, along with the corresponding value of $\sin^2\theta_W = 0.2274$ [13].

Table 4: Theoretical prediction of cross sections for different structure function sets

SF set	Λ_{QCD} (MeV)	σ_W (nb)	σ_Z (nb)	σ_W/σ_Z
HMRSB	190	6.59	2.02	3.26
KMRSB	190	6.84	2.10	3.27
HMRSE	100	6.73	2.04	3.30
MT-S1	212	6.52	2.08	3.14
MT-B1	194	6.47	2.04	3.17
MT-E1	155	6.28	2.08	3.03
GRV	200	6.67	2.13	3.13

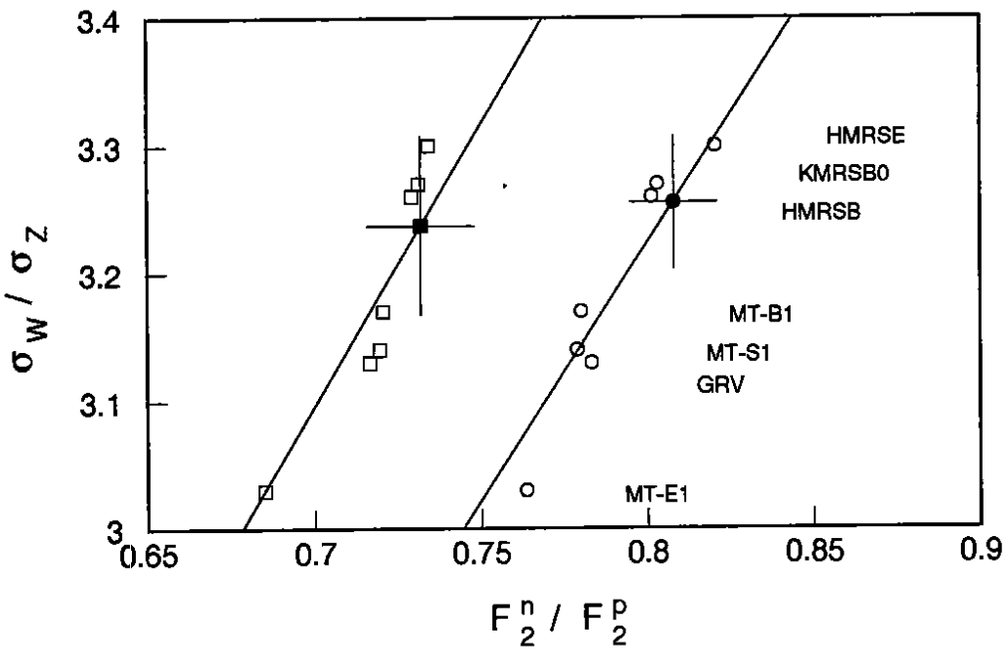

Figure 4: The predictions of σ_W/σ_Z plotted against F_2^n/F_2^p for different structure functions sets (labeled at right). The Q^2 value used to calculate σ_W (σ_Z) is $m_W{}^2$ ($m_Z{}^2$), while the ratio F_2^n/F_2^p has been calculated for $x = 0.125$, $Q^2 = 20.3$ GeV^2 (open circles) and $x = 0.175$, $Q^2 = 24.8$ GeV^2 (open squares). Also shown are the measured NMC values of F_2^n/F_2^p for the same x and Q^2 values (solid points, with their experimental errors as horizontal bars). The vertical coordinates of the solid points show the extrapolated predictions of σ_W/σ_Z (see text).

Although one benefits from cancellation of some theoretical errors in the ratio, there is still some dependence on the boson masses and structure functions. The ratio of partial widths is sensitive to the boson masses and to $\sin^2\theta_W$, but given the experiental bounds on m_W and m_Z the effect on R is only about 0.6% and is neglected. The dominant theoretical error on R results from the structure function dependence of σ_W/σ_Z, which arises from the uncertainty in the ratio, d/u, of parton density functions for down and up valence quarks, since W and Z bosons couple differently to the two types of quarks. The d/u ratio is probed at lower Q^2 by the F_2^n/F_2^p measurement in deep inelastic scattering experiments, and the recent data from the NMC experiment [21] can be exploited to restrict the range of σ_W/σ_Z. As shown in Fig. 4, there is a strong correlation between the σ_W/σ_Z predictions for different structure function sets and the corresponding predictions of F_2^n/F_2^p, which are calculated for $x = 0.125$, $Q^2 = 20.3$ GeV^2 and $x = 0.175$, $Q^2 = 24.8$ GeV^2 (the two values of x have been chosen because they fall in the relevant range for W and Z production at $\sqrt{s} = 630$ GeV, $0.1 \lesssim x \lesssim 0.2$). The fit lines in Fig. 4 are simple estimates of the relations between σ_W/σ_Z and F_2^n/F_2^p at the two x values. The horizontal position and error bars of the solid points show the measured values and statistical errors of F_2^n/F_2^p (the systematic errors are negligible), while the vertical coordinate shows the corresponding value and error for σ_W/σ_Z derived from the linear relations shown. The two points are combined to give $\sigma_W/\sigma_Z = 3.26\pm0.07\pm0.05$ where the first error is propagated from the experimental errors on F_2^n/F_2^p, and the second error corresponds to the systematic uncertainties of the extrapolation, so an overall error of $\pm3\%$ is assigned to the theoretical uncertainties in the calculation of R. This technique for extracting σ_W/σ_Z predictions from F_2^n/F_2^p measurements is described in ref. [22].

In combination with the value of $\Gamma_Z = 2.487 \pm 0.010$ GeV from LEP [20], one obtains

$$\Gamma_W = 2.10 \pm^{0.14}_{0.13} (\text{stat}) \pm 0.06(\text{syst}) \pm 0.06(\text{SF}) \text{ GeV } = 2.10 \pm 0.16 \text{ GeV} \qquad (7)$$

Similar measurements have been reported by CDF [23] and UA1 [24]. Using the R values reported by these experiments along with the same theoretical inputs used in the UA2 measurement, one has ${\Gamma_W}^{CDF} = 2.20 \pm 0.16$ GeV (electrons and muons combined) and ${\Gamma_W}^{UA1} = 2.19 \pm 0.30$ GeV (muons) [25].

The total width Γ_W is sensitive to any decay modes of the W whether they are detected or not. In particular, the presence of a top quark lighter than the W would result in a larger width, so Γ_W can be used to set a lower limit on m_{top}. The best direct search for the top quark restricts its mass to $m_{top} > 89$ GeV [26]. This limit, however, requires that the top has the expected semileptonic branching ratio and could be invalid, for example, if the top decays via a charged Higgs boson. Apart from Γ_W measurements, the best limits on m_{top} which do not depend on the decay modes of the top come from LEP, and establish a limit well below m_W: $m_{top} > 46$ GeV [27]. Figure 5 shows the prediction for Γ_W as a function of m_{top} including mass dependent QCD corrections [28]. From the UA2 measurement of the width alone, one obtains a limit of $m_{top} > 53$ GeV at the 95% confidence level. The combination of UA2, CDF, and UA1 gives $\Gamma_W = 2.15\pm0.11$ which corresponds to $m_{top} > 55$ GeV at the 95% CL.

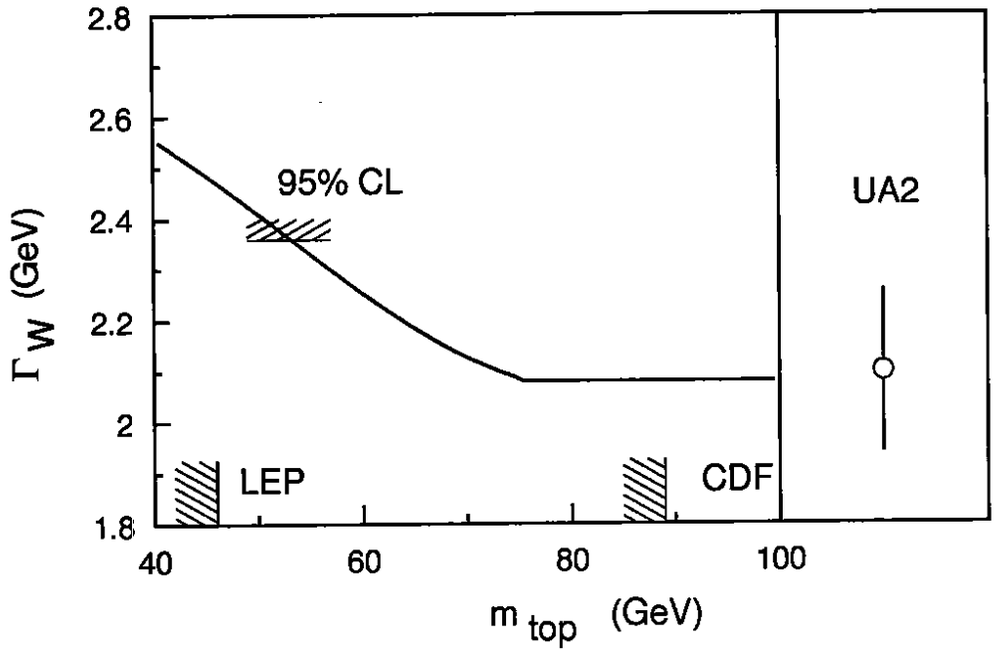

Figure 5: The final result for Γ_W is compared with the Standard Model predictions for Γ_W as a function of m_{top}.

6 Conclusions

The final data sample of the UA2 experiment at the CERN $\bar{p}p$ collider has been used to measure the rates for W and Z production followed by decays including electrons. The results $\sigma_W^e = 682 \pm 12 \pm 40$ pb and $\sigma_Z^e = 65.6 \pm 4.0 \pm 3.8$ pb are in good agreement with $O(\alpha_s^2)$ predictions if the top quark is heavier than the W. The ratio of cross sections has been used to extract the total width of the W, $\Gamma_W = 2.10 \pm 0.16$ GeV. This in turn gives a limit on the mass of the top quark which does not depend on any assumptions about its decay modes: $m_{top} > 53$ GeV at the 95% confidence level.

Acknowledgements

The technical staff of the institutes collaborating in UA2 have contributed substantially to the construction and operation of the experiment. We deeply thank them for their continuous support. The experiment would not have been possible without the very successful operation of the improved CERN $\bar{p}p$ Collider, whose staff and coordinators we sincerely thank for their collective effort.

Financial support from the Schweizerischen Nationalfonds zur Förderung der Wissenschaftlichen Forschung to the Bern group, from the UK Science and Engineering Research Council to the Cambridge group, from the Bundesministerium für Forschung und Technologie to the Dortmund and Heidelberg groups, from the Australian Research Council, the CRA Pty Ltd, and the Victorian Education Foundation to the Melbourne group, from the Institut National de Physique Nucléaire et de Physique des Particules to the Orsay group, from the Istituto Nazionale di Fisica Nucleare to the Milano, Pavia, Perugia and Pisa groups and

from the Institut de Recherche Fondamentale (CEA) to the Saclay group are acknowledged.

References

[1] UA2 Collab., J. Alitti *et al.*, *Z. Phys.* **C47** (1990) 11.

[2] R. Hamberg, W. L. Van Neerven, and T. Matsuura, *Nucl. Phys.* **B359** (1991) 343.

[3] A. Beer *et al.*, *Nucl. Instr. and Meth.* **A224** (1984) 360.

[4] R. Ansari *et al.*, *Nucl. Instr. Meth.* **A279** (1989) 388.

[5] F. Bosi *et al.*, *Nucl. Instr. Meth.* **A283** (1989) 532.

[6] R. Ansari *et al.*, *Nucl. Instr. Meth.* **A263** (1988) 51.

[7] R.E. Ansorge *et al.*, *Nucl. Instr. Meth.* **A265** (1988) 33;
J. Alitti *et al.*, *Nucl. Instr. Meth.* **A279** (1989) 364.

[8] K. Borer *et al.*, *Nucl. Instr. Meth.* **A286** (1990) 128.

[9] UA2 Collab., J. Alitti, *et al.*, *Phys. Lett.* **B263** (1991) 563.

[10] UA4 Collab., D. Bernard *et al.*, *Phys. Lett.* **B198** (1987) 583.

[11] U. Amaldi *et al.*, *Phys. Lett.* **B66** (1977) 390;
A. Martin, *Proceedings of the Workshop on $\bar{p}p$ Collider Physics* (Bern 1984) 308.

[12] F.A. Berends and R. Kleiss, *Z. Phys* **C27** (1985) 365;
F.A. Berends, R. Kleiss, J.P. Revol, and J.P. Vialle, *Z. Phys.* **C27** (1985) 155.

[13] UA2 Collab., J. Alitti, *et al.*, *An Improved Determination of the Ratio of W and Z masses at the CERN $\bar{p}p$ Collider,* CERN-PPE/91-163, accompanying letter. The measurement is $m_W = 80.35 \pm 0.37$ GeV.

[14] P.N. Harriman, A.D. Martin, R.G. Roberts, and W.J. Stirling, *Phys. Rev.* **D42** (1990) 798;
Phys. Lett. **B243** (1990) 421.

[15] H. Plothow-Besch, *Parton Density Functions*, Proceedings of the 3rd Workshop on Detector and Event Simulation in High Energy Physics (Amsterdam, April 1991).

[16] J. Kwiecinski, A.D. Martin, R.G. Roberts and W.J. Stirling, *Phys. Rev.* **D42** (1990) 3645.

[17] M. Glück, E. Reya and A. Vogt, Dortmund preprint DO-TH 91/07 (1991).

[18] J.G. Morfín and W.K. Tung, Fermilab Preprint Fermilab-PUB-90/74.

[19] CDF Collab., F. Abe, *et al.*, *Phys. Rev. Lett.* **65** (1990) 2243;
Phys. Rev. **D43** (1991) 2070.

[20] J. Carter, summary talk at Lepton-Photon Symposium and Int. Europhysics Conference on High Energy Physics (Geneva, July-August 1991).

[21] NM Collab., D. Allasia, *et al.*, *Phys. Lett.* **249B** (1990) 366.

[22] P. Colas, D. Denegri and C. Stubenrauch, *Z. Phys.* **C40** (1988) 527.

[23] CDF Collab., F. Abe, *et al.*, *Phys. Rev. Lett.* **64** (1990) 152.

[24] UA1 Collab., C. Albajar, *et al.*, *Phys. Lett.* **253B** (1991) 503.

[25] H. Plothow-Besch, mini-rapporteur talk at Lepton-Photon Symposium and Int. Europhysics Conference on High Energy Physics (Geneva, July-August 1991).

[26] K. Sliwa, in *High Energy Hadron Interactions*, proceedings of the XXVth Rencontres de Moriond, Les Arcs, France, edited by J. Tran Thanh Van (Editions Frontieres, Gif-sur-Yvette, 1990).

[27] ALEPH Collab., D. Decamp *et al.*, *Phys. Lett.* **236B** (1990) 511;
DELPHI Collab., P. Abreu *et al.*, *Phys. Lett.* **242B** (1990) 536;
OPAL Collab., M.Z. Akrawy *et al.*, *Phys. Lett.* **236B** (1990) 364.

[28] T. Alvarez, A. Leites and J. Terrón, *Nucl. Phys.* **B301** (1988) 1.